Role of the surface states in the magnetotransport properties of ultrathin bismuth films

N. Marcano,[1,2,3] S. Sangiao,[1,2,4] C. Magén,[1,5] L. Morellón,[1,2,4] M. R. Ibarra,[1,2,4] M. Plaza,[6] L. Pérez,[7] and J. M. De Teresa[1,2]

[1]*Departamento de Física de la Materia Condensada, Universidad de Zaragoza, 50009 Zaragoza, Spain*

[2]*Instituto de Ciencia de Materiales de Aragón, CSIC-Universidad de Zaragoza, 50009 Zaragoza, Spain*

[3]*Centro Universitario de la Defensa, Academia General Militar Crta. de Huesca s/n, 50090 Zaragoza, Spain*

[4]*Instituto de Nanociencia de Aragón, Universidad de Zaragoza, 50018 Zaragoza, Spain*

[5]*Laboratorio de Microscopías Avanzadas, Instituto de Nanociencia de Aragón-ARAID, Universidad de Zaragoza, 50018 Zaragoza, Spain*

[6]*Departamento de Física de Materia Condensada, Universidad Autónoma de Madrid, 28049 Madrid, Spain*

[7]*Departamento de Física de Materiales, Universidad Complutense de Madrid, 28040 Madrid, Spain*

We have investigated the magnetotransport properties of ultrathin films of Bi grown on thermally oxidized Si(001) substrates with thickness ranging from 10 to 100 nm at temperatures down to 2 K and in magnetic fields up to 90 kOe. Remarkable differences both in temperature and field dependence of the Hall resistivity are found for the films with thickness above and below 20 nm. These observations can be explained due to the presence of surface states, which play an important role in determining the electronic transport properties of the thinnest films. The estimated surface carrier density 4×10^{13} cm^{-2} at room temperature correlates well with that recently reported from angle-resolved photoemission spectroscopy on ultrathin Bi(001) films.

I. INTRODUCTION

Semimetal bismuth (Bi) is one of the most studied elements in solid-state physics because of its unique electronic properties due to its complex and highly anisotropic Fermi surface. The elongated pockets of holes and electrons with small effective masses lead to a large Fermi wavelength (λ_F) of about 30 nm, which is more than a factor of 100 larger than in regular metals. Moreover, the mean-free path in Bi can be as much as several millimeters,[1] several orders of magnitude larger than those for most metals. These characteristics make Bi a suitable candidate to study both classical and quantum size effect (QSE), for which the characteristic lengths are the carrier mean-free path and Fermi wavelength, respectively. In the 1960s, the oscillation of the film resistance with the film thickness t was reported[2] and a semimetal-to-semiconductor transition caused by QSE was predicted at a critical thickness of $t \approx 30$ nm.[3]

However, after three decades of intensive research, whether such phenomena can really be observed has been argued and it is still a controversial issue.[4–6] Those predictions were based on the bulk band structure but recent experiments have revealed the significant contribution from the surface band as the system downsizes to nanometer scale, making this system even more intriguing. In fact, one remarkable effect of the surface in semiconductors is the appearance of surface states with energy levels in the gap between valence and conduction bands.[7] The schematic energy band diagram showing the energies of the band edges and the Fermi level for bulk Bi and the tentative energy band scheme for ultrathin Bi films is presented in Fig. 1. One could speculate that the Bi surface band could be responsible for the transport properties of Bi films and nanowires when the thickness is below 20–30 nm, once the bulk bands have been pushed away from the Fermi level due to size effects. Thus, the conduction might be confined typically within one monolayer at the film surface, opening a rich physics to explore, as in the case of topological insulators.[8] Thus, it seems pertinent to investigate such possibility.

To date, evidences of metallic surface states have been found in different bismuth systems. Superconductivity in granular systems built from Bi clusters where related to the strongly increased surface density of states.[9] Direct observations by means of angle-resolved photoemission spectroscopy (ARPES) show that the surface states of Bi crystals are highly metallic in contrast to the semimetallic nature of bulk Bi, with carrier densities of $\Sigma \sim 2$–5×10^{12} cm^{-2}.[10–13] Hirahara *et al.*[14] provided evidence of large surface-state conductivity at room temperature in ultrathin Bi(001) films via *in situ* microscopic-four-point probe conductivity measurements, concluding that transport properties are dominated by these inert surface states that are Rashba spin split.[15,16]

So far, there have been magnetotransport studies of very thin films that showed the presence of an excess carrier density of thin films of Bi.[17,18] Those studies, however, were focused on thin films with thickness larger than λ_F. In this paper, we report on a detailed study of the magnetoresistance
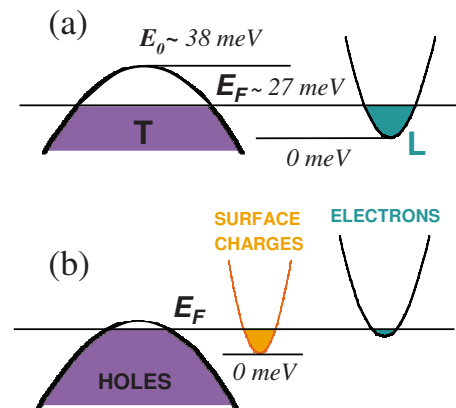

FIG. 1. (Color online) Schematic energy-band diagram showing the energies of the band edges for the L-point electron pockets and the T-point holes and the Fermi level for (a) bulk Bi, where the band overlap is 38 meV and Fermi level is 27 meV from the bottom of the L-point pocket band edge, and (b) tentative energy-band scheme for ultrathin Bi films (see text).

(MR) and Hall resistivity of ultrathin Bi films grown on thermally oxidized Si(001) with thickness ranging from 10 to 100 nm, for which we observe a remarkable change both in the temperature and magnetic field dependence at the thickness crossover of 20 nm. Our results pinpoint the key role played by the surface states in the transport properties when the system downsizes below λ_F.

II. EXPERIMENTAL

The Bi ultrathin films, 10–100 nm, were grown on Si(001) substrates by e-beam evaporation in vacuum at a pressure of 10^{-7} Torr at a deposition rate of 0.5 nm/min. Film thickness was controlled with a quartz crystal microbalance. Prior to the Bi evaporation, 200 nm-thick SiO_2 was formed on top of the Si substrate through thermal oxidation. The crystalline quality, microstructure and thickness of the samples were checked by high-resolution x-ray diffraction (XRD) and x-ray reflectivity (XRR), scanning electron microscopy (SEM) and ultrahigh-resolution transmission electron microscopy (HRTEM). XRD were performed in a D8 Advanced Bruker diffractometer and the used wavelength was that of Cu $K\alpha_1$. HRTEM experiments have been carried out in a FEI Titan Cubed TEM equipped with an image aberration corrector and operated at 300 kV. Scanning transmission electron microscopy (STEM) combined with electron energy loss spectroscopy (EELS) and energy dispersive x-ray spectroscopy (EDX) have been performed in the FEI Titan TEM equipped with a probe corrector, a Gatan Tridiem 866 ERS energy filter and an EDAX x-ray spectrometer and operated at 300 kV. The lamella for the cross-sectional TEM study has been fabricated in a FEI Helios 600 Nanolab with the ion column operated at 5 kV. MR and Hall effect were carried out in a commercial PPMS from Quantum Design by means of conventional four-contact technique. The samples were patterned by a two-step optical lithography process in order to have a well-defined geometry for the transport measurements.[19] The lateral size of the typical electrode for the flow of the current was 4 μm and titanium pads were patterned for the measurements of the voltage drop. In all measurements, the magnetic field H was applied perpendicular to the film plane and the current flow was within the film plane, parallel to the substrate edge. To cancel the effect of the field on the longitudinal component of the resistivity contributing to the measured voltage, we swept the field to positive values and then to negative values and defined the Hall signal as half the difference between the signals measured at positive and negative fields.

III. RESULTS AND DISCUSSION

Figure 2(a) shows the $\theta/2\theta$ x-ray diffraction pattern obtained for the Bi 100 nm-thick films at room temperature as representative of the structural analysis. Bismuth has a rhombohedral crystal structure, which is usually described in a hexagonal system. The films used in this work are polycrystalline but strongly textured as evidenced by strong (003), (006), and (009) peaks which indicates that the Bi grains preferentially grow with the trigonal axis [001] perpendicular
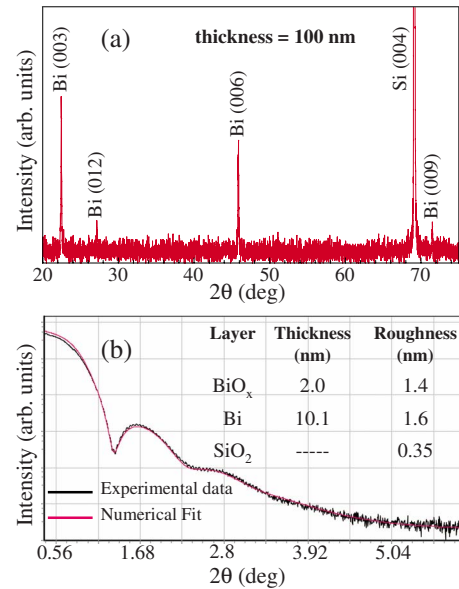

FIG. 2. (Color online) (a) X-ray diffraction pattern of the 100-nm Bi film and (b) XRR measurement from the 10-nm thick Bi film and the numerical fit described in the text. The obtained values of thickness and roughness of all layers have been listed as an inset.

to the plane of the film. SEM images reveal that the samples consist of grains with sizes comparable to the film thickness (i.e., ranging from 10 to 100 nm). Film thickness has been determined by XRR measurements. Figure 2(b) shows XRR measurements for the 10 nm-thick Bi film. The thickness and roughness of the layers have been numerically analyzed by means of the commercial software LEPTOS provided by Bruker. From the numerical analysis of the XRR data, the film thickness was found to be 10.1 nm and the roughness of the layer 1.6 nm. A layer of Bi oxide (2 nm thick and the roughness of the layer 1.4 nm) needs to be considered in order to reproduce the experimental data.

HRTEM images on 10-nm film, as representative of this study, reveal the crystal structure and morphology of the Bi thin films, as illustrated in Fig. 3. The film has polycrystalline nature textured with the (001) trigonal direction out of plane and is composed of flat nanocrystals about 10–12 nm thick and elongated along the growth plane. An example of one of these grains is displayed in Fig. 3(a) whereas Fig. 3(b) plots the Fast Fourier Transform of the area of the image where the grain is, showing that the crystal symmetry and lattice reflections match those of hexagonal Bi oriented along
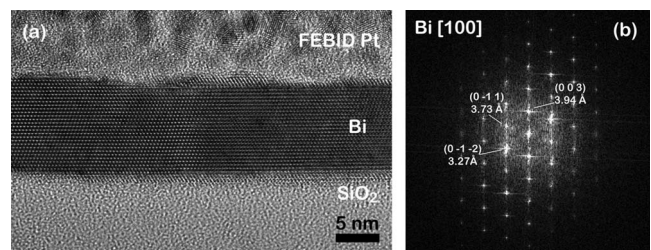

FIG. 3. (a) HRTEM image of Bi thin film grown on SiO_2 layer and capped with a FEBID Pt protective layer. (b) FFT of the Bi film showing the crystal symmetry and the main lattice periodicities.
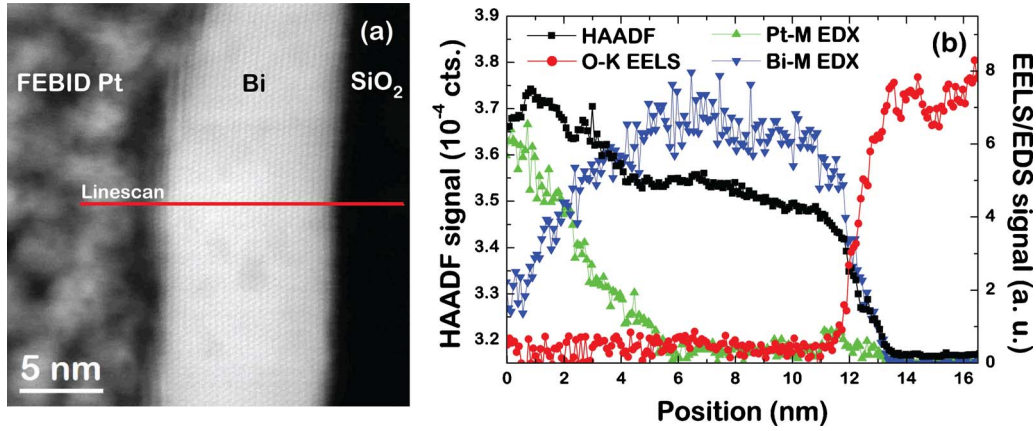
FIG. 4. (Color online) (a) HAADF STEM image of Bi thin film used as a reference image for EELS-EDX linescan. (b) Integrated EELS and EDX signals corresponding to the O K edge (EELS), and the Bi M and Pt M edge (EDX). HAADF signal acquired simultaneously to the spectrum profile is also represented.

the [100] axis. Relatively rough interfaces with the SiO$_2$ buffer and with the focused electron beam induced deposit of Pt used as a protective layer during lamella preparations cause some contrast intermixing which makes impossible to determine the nature of the interfaces and the interface with the substrate. To clarify this point, STEM-EELS/EDX experiments have been performed to characterize the chemical composition of the surface of the films. Figure 4(a) shows the high angle annular dark field (HAADF) STEM image of one of the grains, showing features similar to those already deduced from the HRTEM experiments. Using this image as a reference, an EELS and EDX spectrum image have been collected along the line in Fig. 4(a). Figure 4(b) displays the profile of EELS oxygen integrated signal extracted from the background substracted O K edge, the integrated signal of EDX Pt M and Bi M edges, and the simultaneously acquired HAADF signal. Several conclusions can be extracted from this linescan. First, the oxygen signal is concentrated in the SiO$_2$ layer and abruptly decreases to noise level at the interface with the Bi layer. No oxygen is observed in the upper surface, the one in contact with the Pt layer, so we can conclude that Bi is metallic with negligible surface oxidation. In addition, Bi surface presents a higher roughness than the interface with the buffer, as can be noticed from the sharper O and Bi profiles of the latter interface with respect to the Pt and Bi profiles at the surface of the Bi film. We need to underline that the Bi M edge chosen to make the profile overlaps in energy with other Pt edges, so the Bi signal does not go to zero at the Pt protective layer whereas the Pt M peak is not overlapped with other elements signal. It is intriguing that the interface of the Bi grain is not oxidized according to the TEM images whereas the x-ray reflectivity measurements indicate an average 2 nm-BiO$_x$ layer in the film. One possible explanation is that some Bi grains are oxidized whereas other ones are not. Another explanation can be that the high-vacuum atmosphere of the TEM experiments tend to remove the oxide layer.

Figures 5(a) and 5(b) show the Hall resistivity (ρ_{Hall}) isotherms from room temperature down to 2 K for the Bi films with thicknesses $t=10$ and 100 nm as representative of the present study. According to the observed temperature and

field dependence the films can be divided into two groups: (i) films with $t \gtrsim 20$ nm, where ρ_{Hall} is not linear with field, changing its sign from negative at room temperature into positive below ~ 100 K and (ii) films with $t < 20$ nm, where ρ_{Hall} displays a linear field dependence remaining its sign negative for the whole temperature range. The remarkable change both in the magnitude and the field dependency of ρ_{Hall} with film thickness is illustrated in Fig. 6, in which ρ_{Hall}
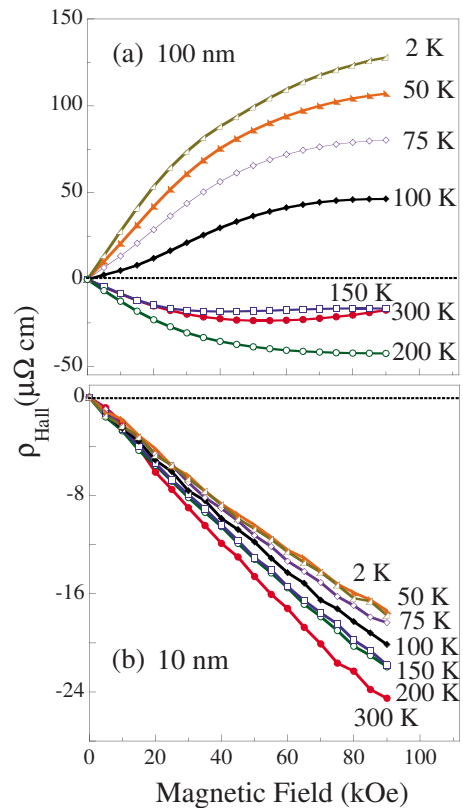

FIG. 5. (Color online) Hall resistivity ρ_{Hall} isotherms at selected temperatures in the 2 to 300 K range for the sake of clarity as a function of magnetic field for (a) $t=100$ nm and (b) $t =10$ nm-thick Bi films as representative samples of the present study. Solid lines drawn are guide to the eyes.
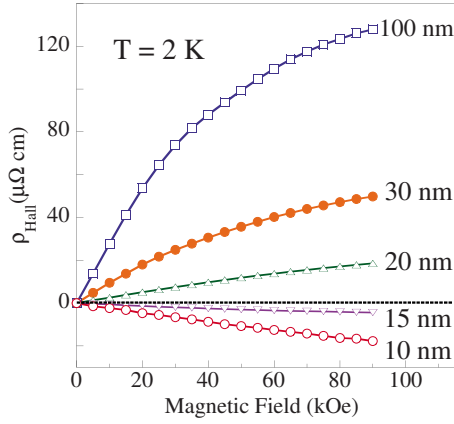
FIG. 6. (Color online) Hall resistivity ρ_{Hall} as a function of magnetic field for several film thickness in the 10 to 100 nm range as representative of this study at 2 K. Solid lines drawn are guide to the eyes.

as a function of magnetic field is compared for different film thickness down to 10 nm at 2 K.

The observation of a linear Hall effect in the 10 nm-thick film from 0 to 90 kOe in the whole temperature range is particularly remarkable. One expects the surface carriers to become important or even a clear majority as film thickness is reduced due to the large surface area per unit volume. Furthermore, finite size or quantum effects in ultrathin films can shift the position of the electron and hole bulk bands, leading to even greater relevance of the surface band. Indeed, according to our analysis, the carrier concentration of the surface band n_s increases with respect to the bulk bands as the thickness of the film is reduced.

In the following, we use the conventional theory of multi-band transport[20] to extract the electron and hole carrier densities and mobilities from a simultaneous fitting of the temperature and field evolution of the MR and Hall resistivity ρ_{Hall}. According to such a model, each band has two parameters, resistivity ρ_i and Hall coefficient $R_i = 1/q_i n_i$ where $q_i = \pm e$ is the charge of the carrier. Each band contributes to the conductivity of the system in parallel with the other bands. Thus, the total conductivity is a sum of the contributions from all the bands $\hat{\sigma} = \Sigma_{i=1} \hat{\sigma}_i$ and the total resistance is $\hat{\rho} = \hat{\sigma}^{-1}$. It should be pointed out that this model does not provide the complete description of the system since the anisotropy in the electron mobilities found in bulk Bi is not being taken into account. Such an effect can have a minor role in our Bi films as they are not single crystalline. This is why we restrict the model to the interplay of three isotropic bands, which in fact provides a good fit to the experimental data.

Figure 7 shows the magnetic field dependence of the resistance $[\rho(H) - \rho(H=0)]$ and ρ_{Hall} at a selected temperature $T = 50$ K for film thickness $t = 10$, 30, and 100 nm as representative of this study. These results have been fitted to the above mentioned model. In agreement with earlier analysis of the magnetotransport properties of 300 nm-thick Bi(001) films we started with a simple two-band model, with a bulk electron and a bulk hole band.[21] In that case, the nonlinear magnetic field dependence of the Hall resistivity was ex-
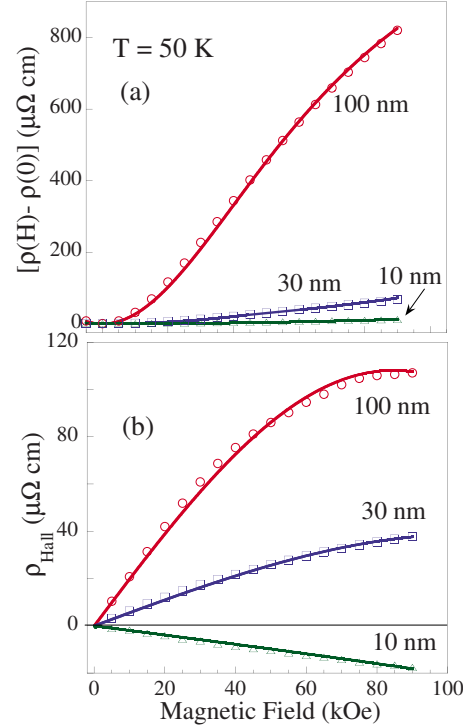

FIG. 7. (Color online) (a) Magnetoresistance (top panel) and Hall resistivity ρ_{Hall} (bottom panel) versus applied field at selected temperature $T = 50$ K for Bi films with thickness $t = 100$, 30, and 10 nm as representative of this study. The solid lines are determined by a fitting procedure that simultaneously includes both sets of data into a three-band model described in the text.

plained by the noncompensated electron and hole bulk bands. This attempt is shown in Fig. 8, which displays the magnetic field dependence of the resistance and ρ_{Hall} at 50 K only for 100 nm-thick film for the sake of clarity. Black solid line is calculated from two band model. It is clear that, in the present study, the inclusion of a third carrier band (with ρ_s and $R_s = 1/en_s$ as characteristic band parameters) is required to account for the temperature and field evolution of the magnetoresistance and ρ_{Hall} (red solid line). We fit MR and ρ_{Hall} simultaneously by adjusting the six parameters (n, p, R_n, R_p, n_s, and R_s) independently, until differences between the fitting curves and the experimental data are minimized. The solid lines in Figs. 7(a) and 7(b) are calculated from our three-band model analysis. The experimental and calculated resistances are in very good agreement for the whole magnetic field range.

For the 100 nm-thick film we obtain $n \approx p \approx 5 \times 10^{18}$ cm^{-3} over 100 K $\leq T \leq$ 300 K temperature range. Those values are in agreement with those reported for 100 nm-thick Bi epitaxial films.[4,17,22] It is worth noting that the three-band model with electron and hole bulk bands together with a minority surface electron band have been recently reported to describe the magnetotransport properties on 100 nm-width Bi nanowires.[23] In the present case, however, the third band can be interpreted as an effective band which contains surface carriers characterized by an effective density and an effective mobility. This model accounts for two possible scenarios: (i) surface electron and hole bands where
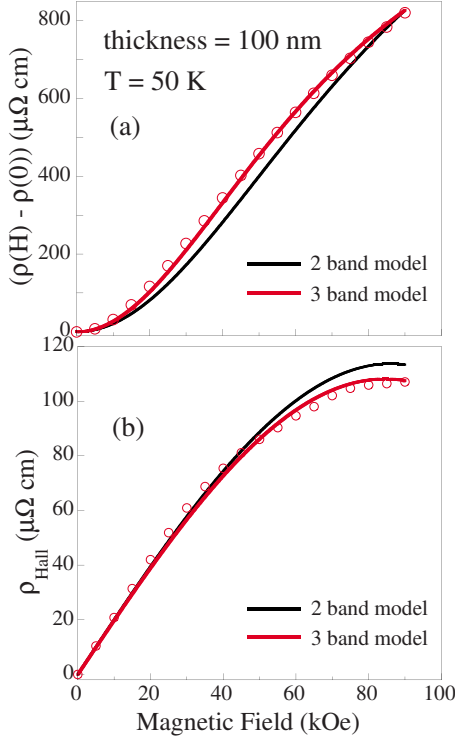
FIG. 8. (Color online) (a) Magnetoresistance (top panel) and Hall resistivity ρ_{Hall} (bottom panel) versus applied field at selected temperature $T=50$ K for Bi films with thickness $t=100$ nm. The solid lines are determined by a fitting procedure that simultaneously includes both sets of data into a two-band (black line) and a three-band model (red line) described in the text.

concentrations of electrons and holes are compensated, or (ii) dominant electron situation with higher mobility than holes. Both possibilities can account for the experimental data presented in this work. Unfortunately, the present measurements do not allow us to discern between them. The present study allows the analysis of the evolution of the ratio of n_s to bulk electrons or holes (n,p) with film thickness. For the 30 nm film, such a ratio is ~ 2 at 2 K whereas it increases up to ~ 5 at 2 K for the 10 nm-thick film. For the latter, we obtain n_s $=4 \times 10^{19}$ cm^{-3} at room temperature. The surface charge per unit area Σ estimated as $n_s \times t$ gives rise to $\Sigma \sim 4 \times 10^{13}$ cm^{-2} in rough agreement with the Σ determined via ARPES measurements for ultrathin Bi(001) films.[14] The mo-

bility $\mu_i = 1/n_i q_i R_i$ and the carrier density n_i for each band obtained from fits to the three band model for the 100 nm, 30 nm, and 10 nm-thick films for selected temperatures (T $=5$ K and $T=50$ K) are listed in Table I. For the 10 nm-thick film the low-temperature magnetoresistance ($T \leq 5$ K) presents an extra contribution coming from the localization effects (weak antilocalization)[24] which has been taken into account in the corresponding analysis.

It is worth noting that in spite of the simplicity of the multiband model, this analysis has been successful in describing the field-dependent resistivity and hall resistivity observed in this work. This approach has enable us to obtain the temperature dependence of the electron and hole densities in each sample and to identify the presence of surface carriers which play a remarkable role in determining the magnetotransport properties of the 10-nm thick film. Such surface carriers are expected to become a clear majority and thus, dominate the electronic transport in ultrathin Bi films as thickness decreases, once the bulk bands have been shifted with respect to the Fermi level due to size effects. In fact, *in situ* micro-four-point-probe measurements showed that the room temperature properties of 2 nm-thick films were dominated by the surface states and not by the states inside the film.[14] Unfortunately, our attempts to grow continuous films with such low thickness were not successful.

The attribution of the third band to surface states is strongly supported by the estimated surface carrier density which is in rough agreement with the Σ determined via ARPES in ultrathin Bi (001) films made in deposition under ultrahigh vacuum on *in situ* cleaned Si surfaces.[14] However, the presence of an impurity band coming from the Bi/SiO$_2$ interface or the film surface Bi/BiO$_x$ can be considered as another plausible scenario which would account for the presence of extra carriers in our films. Although the STEM-EELS/EDX experiments indicate the high quality of the films and the interfaces, as well as the absence of Bi oxide on the surface, further experiments beyond the scope of the present manuscript would be required to discern between both scenarios.

IV. CONCLUSIONS

The thickness and temperature dependence of the magnetoresistance and Hall effect in ultrathin Bi films have been studied and analyzed according to the multiband model. We

TABLE I. Transport parameters for the 100, 30, and 10 nm-thick films as representative samples of the present study at selected temperatures, $T=5$ K and $T=50$ K, determined by the three-band model analysis described in the text.

Film thickness (nm)	T (K)	p (10^{18}/cm^3)	n (10^{18}/cm^3)	n_s (10^{18}/cm^3)	μ_p (cm^2/V s)	μ_n (cm^2/V s)	μ_{n_s} (cm^2/V s)
100	50	1.74	4.9	9.4	677.5	212.7	139.5
100	5	0.82	5.7	10.2	633.7	131.8	79.5
30	50	7.1	2.8	8.9	630.1	576.1	344.2
30	5	4.5	6.2	8.4	711.2	328.5	292.6
10	50	8.12	13.2	23.6	134.5	91.4	57.2
10	5	7.1	13.9	31.3	35.4	23.7	11.1

show that the remarkable changes observed in the magnetotransport as film thickness is reduced below Fermi wavelength ($t < 30$ nm) can, within the uncertainty outlined above, be interpreted as due to the appearance of surface states, which are found to play an important role in determining the transport properties of these films. Our results indicate that both bulk and surface carriers participate in the conduction process even in the thinnest (10 nm) studied film but with increasing contribution of the surface band as the film thickness decreases. Our results allow one to conclude that ultrathin bismuth films can habilitate the study of electronic effects approaching two-dimensional systems, as occurs in few-layer graphene.

[1] R. Hartman, Phys. Rev. B **181**, 1070 (1969).

[2] Yu. F. Ogrin, V. N. Lutskii, and M. I. Elison, JETP Lett. **3**, 71 (1966).

[3] V. B. Sandomirskii, Sov. Phys. JETP **25**, 101 (1967).

[4] C. A. Hoffman, J. R. Meyer, F. J. Bartoli, A. Di Venere, X. J. Yi, C. L. Hou, H. C. Wang, J. B. Ketterson, and G. K. Wong, Phys. Rev. B **48**, 11431 (1993).

[5] H. T. Chu, Phys. Rev. B **51**, 5532 (1995).

[6] E. I. Rogacheva, S. N. Grigorov, O. N. Nashchekina, S. Lyubchenko, and M. S. Dresselhaus, Appl. Phys. Lett. **82**, 2628 (2003).

[7] K. Seeger, *Semiconductor Physics* (Springer-Verlag, Wien, 1973).

[8] D. Hsieh, D. Qian, L. Wray, Y. Xia, Y. S. Hor, R. J. Cava, and M. Z. Hasan, Nature (London) **452**, 970 (2008).

[9] B. Weitzel and H. Micklitz, Phys. Rev. Lett. **66**, 385 (1991).

[10] C. R. Ast and H. Höchst, Phys. Rev. Lett. **87**, 177602 (2001).

[11] Yu. M. Koroteev, G. Bihlmayer, J. E. Gayone, E. V. Chulkov, S. Blugel, P. M. Echenique, and Ph. Hofmann, Phys. Rev. Lett. **93**, 046403 (2004).

[12] T. Hirahara, T. Nagao, I. Matsuda, G. Bihlmayer, E. V. Chulkov, Yu. M. Koroteev, P. M. Echenique, M. Saito, and S. Hasegawa, Phys. Rev. Lett. **97**, 146803 (2006).

[13] Ph. Hofmann, Prog. Surf. Sci. **81**, 191 (2006).

[14] T. Hirahara, I. Matsuda, S. Yamazaki, N. Miyata, S. Hasegawa, and T. Nagao, Appl. Phys. Lett. **91**, 202106 (2007).

[15] T. Hirahara, K. Miyamoto, I. Matsuda, T. Kadono, A. Kimura, T. Nagao, G. Bihlmayer, E. V. Chulkov, S. Qiao, K. Shimada, H. Namatame, M. Taniguchi, and S. Hasegawa, Phys. Rev. B **76**, 153305 (2007).

[16] T. Hirahara, K. Miyamoto, A. Kimura, Y. Niinuma, G. Bihlmayer, E. V. Chulkov, T. Nagao, I. Matsuda, S. Qiao, K. Shimada, H. Namatame, M. Taniguchi, and S. Hasegawa, New J. Phys. **10**, 083038 (2008).

[17] D. L. Partin, J. Heremans, D. T. Morelli, C. M. Thrush, C. H. Olk, and T. A. Perry, Phys. Rev. B **38**, 3818 (1988).

[18] C. A. Hoffman, J. R. Meyer, F. J. Bartoli, A. Di Venere, X. J. Yi, C. L. Hou, H. C. Wang, J. B. Ketterson, and G. K. Wong, Phys. Rev. B **51**, 5535 (1995).

[19] J. M. De Teresa, A. Fernández-Pacheco, L. Morellon, J. Orna, J. A. Pardo, D. Serrate, P. A. Algarabel, and M. R. Ibarra, Microelectron. Eng. **84**, 1660 (2007).

[20] N. W. Ashcroft and N. D. Mermin, *Solid State Physics* (Holt, Rinehart, and Winston, New York, 1976).

[21] N. Marcano, S. Sangiao, J. M. De Teresa, L. Morellón, M. R. Ibarra, M. Plaza, and L. Pérez, J. Magn. Magn. Mater. **322**, 1460 (2010).

[22] Yu. F. Komnik and V. V. Andrievskii, Sov. J. Low Temp. Phys. **1**, 51 (1975).

[23] N. Marcano, S. Sangiao, M. Plaza, L. Pérez, A. Fernández Pacheco, R. Córdoba, M. C. Sánchez, L. Morellón, M. R. Ibarra, and J. M. De Teresa, Appl. Phys. Lett. **96**, 082110 (2010).

[24] S. Sangiao, N. Marcano, L. Morellón, M. R. Ibarra, and J. M. De Teresa (unpublished).